Raman Optical Activity and Circular Dichroism Reveal Dramatic Differences in the Influence of Divalent Copper and Manganese Ions on Prion Protein Folding†

Fujiang Zhu,‡ Paul Davies,§ Andrew R. Thompsett,§ Sharon M. Kelly,|| George E. Tranter,⊥ Lutz Hecht,‡ Neil W. Isaacs,‡ David R. Brown,*,§ and Laurence D. Barron*,‡

WestChem, Department of Chemistry, University of Glasgow, Glasgow G12 8QQ, United Kingdom, Department of Biology and Biochemistry, University of Bath, Bath BA2 7AY, United Kingdom, Institute of Biomedical and Life Sciences, University of Glasgow, Glasgow G12 8QQ, United Kingdom, and Chiralabs Ltd., BCIE, Oxford University Begbroke Science Park, Sandy Lane, Yarnton, Oxfordshire OX5 1PF, United Kingdom

Received November 19, 2007; Revised Manuscript Received December 18, 2007

ABSTRACT: The binding of divalent copper ions to the full-length recombinant murine prion protein PrP^{23-231} at neutral pH was studied using vibrational Raman optical activity (ROA) and ultraviolet circular dichroism (UV CD). The effect of the Cu^{2+} ions on PrP structure depends on whether they are added after refolding of the protein in water or are present during the refolding process. In the first case ROA reveals that the hydrated α-helix is lost, with UV CD revealing a drop from ∼25% to ∼18% in the total α-helix content. The lost α-helix could be that comprising residues 145−156, located within the region associated with scrapie PrP formation. In the second case, ROA reveals the protein's structure to be almost completely disordered/irregular, with UV CD revealing a drop in total α-helix content to ∼5%. Hence, although Cu^{2+} binding takes place exclusively within the unfolded/disordered N-terminal region, it can profoundly affect the structure of the folded/α-helical C-terminal region. This is supported by the finding that refolding in the presence of Cu^{2+} of a mutant in which the first six histidines associated with copper binding to the N-terminal region are replaced by alanine has a similar α-helix content to the metal-free protein. In contrast, when the protein is refolded in the presence of divalent manganese ions, ROA indicates the α-helix is reinforced, with UV CD revealing an increase in total α-helix content to ∼30%. The very different influence of Cu^{2+} and Mn^{2+} ions on prion protein structure may originate in the different stability constants and geometries of their complexes.

Prion proteins are associated with a variety of neurodegenerative diseases, known as transmissible spongiform encephalopathies (TSE) (*1*). Despite much effort, an understanding of some key aspects of TSE disease remains elusive, such as the existence of an infectious form along with genetic and sporadic forms, something that has not been recognized in any other class of neurodegenerative disease. The current model involves conversion of a ubiquitous cellular form of the prion protein (PrP^C) into a scrapie (amyloid fibril) form (PrP^{Sc}), the prion protein being both target and infectious agent. PrP^C has a high proportion of α-helical structure, is soluble in detergents and is susceptible to proteolysis. Conversely, PrP^{Sc} has a high β-sheet content, is insoluble in detergents, and is partially resistant to proteolysis. Further understanding of TSE disease requires more detailed knowledge of the solution structures of prion proteins and the conformational changes associated with the transformation pathways of PrP^C into PrP^{Sc} (*2*, *3*), which in turn will facilitate the rational design of effective anti-TSE compounds (*4*).

PrP^C has between 208 and 220 amino acid residues depending on the particular mammalian species. Early structural analysis by Fourier transform infrared (FTIR)[1] and ultraviolet circular dichroism (UV CD) spectroscopy indicated that PrP^C contains significant amounts of α-helix but little amounts of β-sheet, whereas PrP^{Sc} contains less α-helix but a significant amount of β-sheet (*5*, *6*). Although there have been numerous NMR studies on the solution structure of PrP^C (*7*), X-ray crystallographic studies have been hampered by difficulties in crystallizing the protein. The NMR structures of full-length recombinant prion proteins of different mammalian species all revealed a structured C-terminal globular domain containing mainly α-helical sequences in the form of a compact three-helix bundle, and a long "flexibly disordered" unfolded N-terminal domain of 80−100 amino acids. More recently the crystal structure of an uncomplexed monomeric recombinant prion protein (ovine PrP) has been solved (*8*) and found to be very similar

† This work was supported by the BBSRC, the EPSRC, and the EU (QLK4-CT-2002-02723).

* Address correspondence to these authors. E-mail: bssdrb@bath.ac.uk (D.R.B.); laurence@chem.gla.ac.uk (L.D.B.). Phone: +44 1225 383133 (D.R.B.); +44 141 330 5168 (L.D.B.) Fax: +44 1225 386779 (D.R.B.); +44 141 330 4888 (L.D.B.).

‡ Department of Chemistry, University of Glasgow.

§ University of Bath.

|| Institute of Biomedical and Life Sciences, University of Glasgow.

⊥ Chiralabs, Ltd.

[1] Abbreviations: FTIR, Fourier transform infrared; NLM, nonlinear mapping; PPII, poly(L-proline II); PrP, prion protein; ROA, Raman optical activity; TSE, transmissible spongiform encephalopathy; UV CD, ultraviolet circular dichroism; ICP, incident circular polarization; SCP, scattered circular polarization.

10.1021/bi7022893 CCC: $40.75
Published on Web 01/19/2008

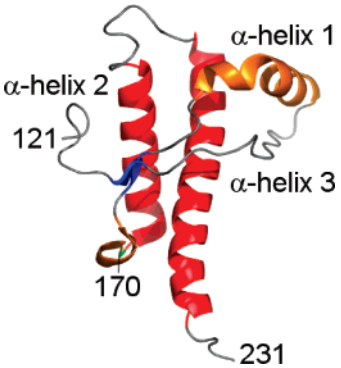

FIGURE 1: Solution NMR structure of murine $PrP^{121-231}$ (PDB code 1xyx). Figure generated with pyMOL (http://www.pymol.org).

to the solution NMR structures of other mammalian species. For crystallization, only the folded C-terminal globular domain $PrP^{128-233}$ was present. It contains 53.8% α-helix, 5.7% 3_{10}-helix, and 3.8% β-strand, with similar values found for the C-terminal domains in the various mammalian NMR solution structures, including that for murine $PrP^{121-231}$ (PDB code 1xyx) illustrated in Figure 1. These values are consistent with α-helix contents of ~25% reported in NMR solution structures of full-length mammalian prion proteins.

PrP^C is a cell surface glycoprotein that is attached to the plasma membrane by a glycosylphosphatidylinositol anchor. This cellular form of the protein binds Cu^{2+}, and it is argued that this copper binding is intimately linked to its normal cellular function in copper transport, sequestration, or antioxidant activity (*9*−*12*). Prion diseases are characterized by a metal imbalance in the brain, associated with loss of copper binding to PrP^C, that occurs simultaneously with conversion of PrP^C to PrP^{Sc} (*13*, *14*). Hence copper binding to PrP is a key factor in considerations of both the normal function of PrP^C and its possible role in TSE disease (*12*). Furthermore, the PrP structure itself might be influenced not only by Cu^{2+} but also by other divalent metal ions such as Mn^{2+} that directly bind to PrP (*15*, *16*). The copper binding appears to be associated with the first six histidines in the unfolded N-terminal region of PrP^C: four Cu^{2+} ions bind to a highly conserved group of octapeptide repeats having the consensus sequence PHGGGWGQ (*17*) with possibly one more taken up in the flexible region between the octarepeats and the globular C-terminal region (*18*, *19*).

Binding of Cu^{2+} establishes turnlike structures, based on paramagnetic square−planar complexes, within the octarepeats (*20*) and also possibly within the region between the octarepeats and the C-terminal region (*19*). However, the paramagnetic nature of Cu^{2+} has so far precluded the use of NMR to obtain the detailed solution structure of the full-length copper-bound protein, so there is currently little information on the overall conformation of the copper-bound N-terminal region and what effect, if any, the binding of Cu^{2+} and other divalent metal ions exerts on the structure of the α-helical C-terminal domain. Here we report a study of this problem using the complementary chiroptical spectroscopic techniques of vibrational Raman optical activity (ROA) and UV CD applied to recombinant murine PrP^{23-231}.

MATERIALS AND METHODS

Production of Recombinant PrP. Tag-free, recombinant prion protein was generated as previously described (*21*). Briefly, a PCR-amplified product consisting of the codons 23−231 of the mouse PrP open reading frame was cloned in the expression vector, pET-23 (Novagen), and transformed into *Escherichia coli* ad494(DE3) or BL21(DE3) strains. Expressed proteins were solubilized by sonication in 8 M urea and recovered by immobilized metal ion affinity chromatography. Columns were charged with copper. The protein was eluted in urea buffer with 300 mM imidazole. The eluted material was treated with 0.5 mM EDTA to ensure the protein was free from leached metal ions. All subsequent steps used doubly deionized water treated with Chelex resin (Sigma) to remove residual metal ions. The denatured protein was refolded by a 10-fold dilution of the urea in deionized water and concentrated by ultrafiltration and two rounds of dialysis to remove residual urea, imidazole and EDTA. Protein concentrations were measured using theoretical extinction coefficients at 280 nm (http://www.us.expasy.org/tools/protparam.html) and confirmed by Bradford assay (Sigma) (*22*). Saturation of the protein with copper or manganese was achieved by the addition of $CuSO_4$ or $MnSO_4$ during the refolding process as previously described (*15*). Incorporation of copper into PrP after refolding was achieved by addition of $CuSO_4$ in the form of a glycine chelate with glycine at a 4-fold molar excess to copper. $Cu(gly)_2$ was added to the protein with a 10-fold molar excess of Cu to PrP. Copper and glycine were removed by dialysis.

For some experiments a mutant of PrP^{23-231} lacking all six N-terminal histidines (i.e., with the mutations H60A, H68A, H76A, H84A, H95A, and H110A) was generated. This mutant (null-his PrP^{23-231}) could not be isolated via its metal affinity as it lacks the metal binding capacity. Therefore an alternative method was used. Pelleted cells expressing the mutant were lysed in lysis buffer (50 mM Tris-HCl pH 7.6, 1 mM EDTA, 100 mM NaCl) containing 4 mg/mL egg lysozyme, 2 mg/mL sodium deoxycholate, and 20 μg/mL bovine pancreas DNase. Lysates were then centrifuged at 10 000*g* for 15 min to pellet protein inclusion bodies and the supernatant discarded. A wash solution containing lysis buffer with 1% IGEPAL 50 and 0.5% Triton X-100 was then used to resuspend the pelleted protein by sonication at 30% maximum power for 1 min. Protein was then repelleted at 10 000*g* for 5 min and the supernatant discarded. This step was repeated six times. A second wash solution of lysis buffer containing 1% Triton X was then used to repeat the six washes as before. The remaining protein was solubilized in binding buffer (8 M urea, 200 mM NaCl, 50 mM Tris-HCl pH 7.6) by sonication at 70% maximum power for three 1-min bursts. Protein purity was confirmed by SDS gel. The null-his mutant PrP was then refolded and dialyzed in the same manner as described for wild-type recombinant PrP.

ROA Spectroscopy. All the murine PrP^{23-231} Raman and ROA spectra reported here were measured in backscattering using the previously described Chiral*RAMAN* instrument manufactured by BioTools, Inc. (*23*), which employs the scattered circular polarization (SCP) measurement strategy (vide infra). The ROA spectra are presented as SCP intensity differences $I_R - I_L$ and the parent Raman spectra as scattered circular polarization intensity sums $I_R + I_L$, where I_R and I_L are the Raman-scattered intensities with right and left circular polarization, respectively.

The proteins were studied at concentrations ~50 mg/mL at ambient temperature (~20 °C) in 10 mM acetate buffer

at pH 6.5. The solutions (~30 μL) were filtered through 0.22 μm Millipore filters into quartz microfluorescence cells, which were centrifuged gently prior to mounting in the ROA instrument. This produced clear solutions showing no evidence of light scattering from aggregation. Residual visible fluorescence from traces of impurities, which can give large backgrounds in Raman spectra, was quenched by leaving the sample to equilibrate in the laser beam for a few hours before acquiring ROA data. Experimental conditions: laser wavelength 532 nm; laser power at the sample, ~500 mW; spectral resolution, ~10 cm^{-1}; acquisition time, ~24 h.

The nonlinear mapping (NLM) analysis of the ROA data was performed using STATISTICA's multidimensional scaling procedures with Euclidean distances in the multidimensional space of standardized spectra (*24*). Specifically, we used monotone nonmetric multidimensional scaling (MS) with spectra standardized to put them all on an equal footing such that each spectrum is shifted and rescaled to have zero mean (so that the ROA band intensities sum to zero) and unit standard deviation.

UV CD Spectroscopy. Far- and near-UV CD spectra were recorded on a Jasco J-810 spectropolarimeter, which was calibrated using a 0.06% w/v solution of ammonium camphor sulfonate (*25*). Spectra were collected in the far-UV region (260−180 nm where possible or 260−190 nm when signal-to-noise ratios were unfavorable, i.e., where the high tension voltage exceeded ~700 V) using a 0.02 cm path length quartz cuvette and murine PrP^{23-231} concentrations of ~0.5−0.7 mg/mL in 10 mM acetate buffer at pH 6.5. Spectra in the near-UV CD region (320 nm-250 nm) were collected using a 0.5 cm path length quartz cuvette and protein concentrations of ~1 mg/mL. Samples were checked for light scattering artifacts due to aggregation by measuring UV spectra between 340 and 240 nm prior to acquiring CD data. With the exception of the sample of null-his PrP^{23-231} refolded without Cu^{2+} (vide infra), the ability to collect good-quality spectra down to 190 nm demonstrated that the samples were indeed free from light-scattering artifacts. The average of eight spectra were collected at 50 nm/min using a 0.5-s response time and a bandwidth of 1.0 nm. In each case the averaged spectra were found to be superimposable on the first spectrum collected. Estimates of protein concentration were obtained using the average values obtained from both UV absorption measurements (using a molar extinction coefficient of 63 370 M^{-1} cm^{-1} at 280 nm) and the Bradford assay (vide supra). Data were corrected to give mean residue weight molar ellipticity values.

Estimates of secondary structure were obtained using the CDSSTR algorithm available from DICHROWEB, an online server hosted by Birkbeck College, University of London (*26*,*27*). CDSSTR is a modification of the Varslc algorithm, which uses the variable selection method to eliminate proteins from the reference set which do not contain characteristics present in the test protein. In each case the NRMSD (normalized root-mean-square deviation) data were used to assess the quality of the fitting procedures: the fits obtained gave NRMSD values less than 0.03 (these values range from 0 for a perfect fit to 1 for no fit).

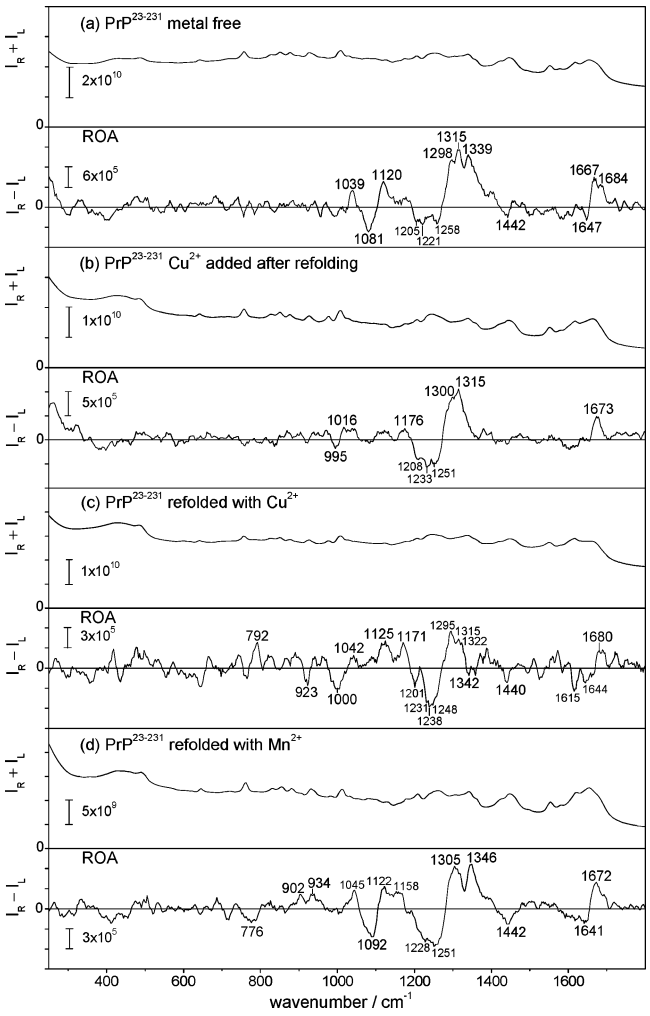

FIGURE 2: Backscattered SCP Raman ($I_R + I_L$) and ROA ($I_R - I_L$) spectra of recombinant murine PrP^{23-231} in aqueous solution: (a) the metal-free water-refolded protein; (b) the metal-free protein refolded in water with the subsequent addition of Cu^{2+} ions; (c) the protein refolded in the presence of Cu^{2+}; (d) the protein refolded in the presence of Mn^{2+}.

RESULTS AND DISCUSSION

ROA Data. ROA measures a small difference in the intensity of vibrational Raman scattering from chiral molecules in right and left circular polarized incident light or, equivalently, the intensity of a small circularly polarized component in the scattered light using incident light of fixed polarization (*28*). The first and second experiments are called *incident circular polarization* (ICP) and SCP ROA, respectively. ROA has been developed to the point where it is an incisive probe of the structure and behavior of biomolecules (*29*), especially proteins (*23*).

Figure 2 shows the backscattered SCP Raman (top of each pair) and ROA (bottom of each pair) spectra of recombinant murine PrP^{23-231} in various states of metal complexation. Detailed vibrational band assignments for protein ROA spectra are provided elsewhere (*23*, *30*, *31*).

The first pair (a) corresponds to the metal-free water-refolded protein. The ROA spectrum is similar to an ICP one previously reported (*32*) for ovine PrP^{25-233}. The most important features to notice for the present study are the positive ROA band at ~1339 cm^{-1} characteristic of hydrated α-helix (as distinct from positive ROA at ~1300 cm^{-1}

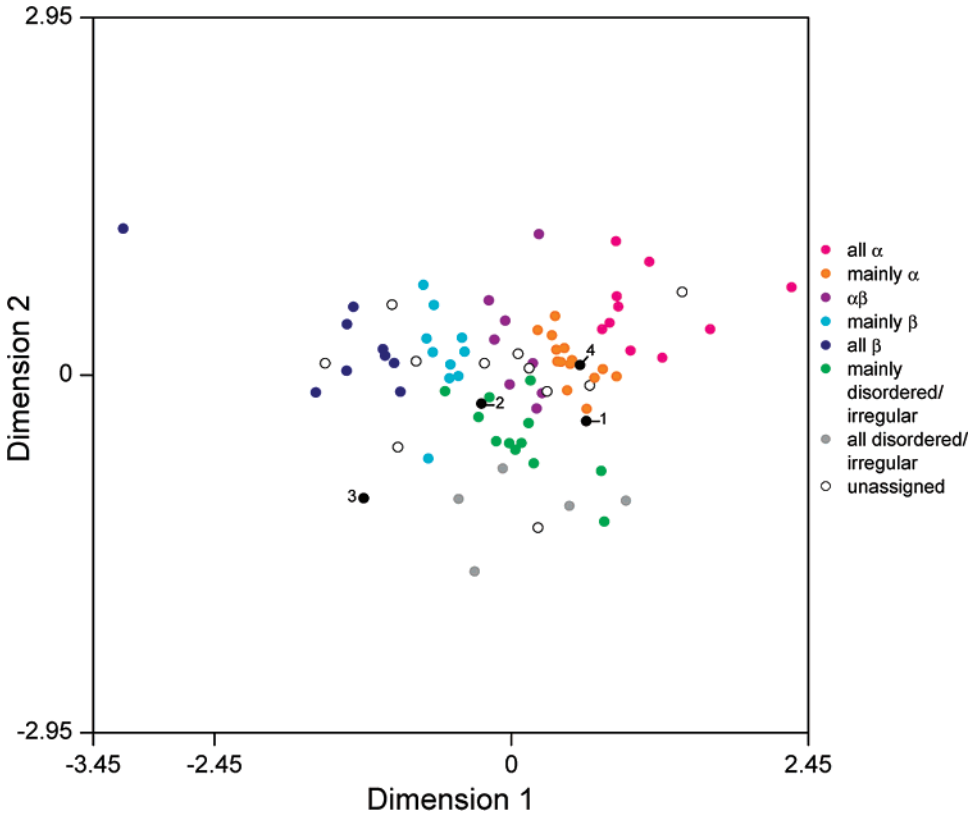

FIGURE 3: Two-dimensional NLM plot of a set of 83 polypeptide, protein, and virus ROA spectra. The samples discussed in the article are labeled as follows: (1) metal-free murine PrP^{23-231} refolded in water; (2) murine PrP^{23-231} refolded in water with subsequent addition of Cu^{2+}; (3) murine PrP^{23-231} refolded in the presence of Cu^{2+}; (4) murine PrP^{23-231} refolded in the presence of Mn^{2+}. More complete definitions of the structural types are: all α, > ~60% α-helix with little or no *β*-sheet; mainly α, >~35% α-helix and a small amount (< ~15%) or no *β*-sheet; α*β*, significant amounts (> ~15%) of both α-helix and *β*-sheet; mainly *β*, > ~35% *β*-sheet and a small amount (< ~15%) or no α-helix; all *β*, > ~45% *β*-sheet with little or no α-helix; mainly disordered/irregular, little α-helix or *β*-sheet; all disordered/irregular, no α-helix or *β*-sheet.

characteristic of unhydrated α-helix) (*31*) and the sharp positive band at ~1315 cm^{-1} characteristic of poly(L-proline) II (PPII) helix (*33*). The earlier study (*32*) also measured the ROA spectrum of the N-terminal truncated ovine protein PrP^{94-233} in which the positive ~1315 cm^{-1} band was completely absent, thereby demonstrating that this band originates in the unfolded N-terminal sequence and also that PPII helix is a significant structural element within it.

The second pair (b) corresponds to murine $PrP,^{23-231}$ again refolded in water, but with the subsequent addition of Cu^{2+} ions, which have induced significant changes in the ROA spectrum. In particular, the positive ~1339 cm^{-1} hydrated α-helix ROA band has completely vanished, together with the distinctive positive−negative−positive ROA band pattern in the range ~1020−1140 cm^{-1}. However, the positive ~1315 cm^{-1} PPII ROA band remains, together with positive intensity at ~1300 cm^{-1} that is characteristic of unhydrated α-helix (*31*).

The third pair (c) corresponds to murine PrP^{23-231} refolded in the presence of Cu^{2+} ions. The ROA spectrum has changed even more dramatically compared with the previous case of addition of Cu^{2+} ions after refolding in water. The overall appearance suggests that very little α-helix or PPII structure remains, with the protein now containing mainly disordered or irregular structure.

The fourth pair (d) corresponds to murine PrP^{23-231} refolded in the presence of Mn^{2+} ions. Unlike the effect of Cu^{2+}, which appears to greatly reduce the content of both α-helix and PPII structure, refolding in the presence of Mn^{2+} appears to significantly increase the α-helix content at the expense of PPII structure, as the characteristic positive PPII ROA band at ~1315 cm^{-1} in the metal-free PrP spectrum (a) has disappeared, with the positive ~1300 and 1340 cm^{-1} α-helix bands now being very prominent. Also the distinctive positive−negative−positive ROA band pattern in the range ~1020−1140 cm^{-1}, observed in the metal-free spectrum (a) but absent from the two copper-bound spectra (b,c), remains highly prominent. Overall, the ROA data suggest that manganese binding has reinforced the α-helix content at the expense of PPII structure, which implies that the additional α-helix may reside in the N-terminal region.

Figure 3 displays a two-dimensional NLM plot of the PrP ROA data in the context of a set of 83 polypeptide, protein, and virus ROA spectra (mostly ICP but some SCP) in aqueous solution over the range 702−1773 cm^{-1} (*34*). A list of the actual polypeptides, proteins, and viruses is provided as Supporting Information to ref 34. NLM is a multivariate analysis technique that starts by regarding each digitized spectrum as a vector from the origin to a point in a multidimensional space, with the axes representing the digitized wavenumbers. Points close to or distant from each other in this multidimensional space are taken to represent similar or dissimilar spectra, respectively. NLM creates a lower dimensional space (two dimensions here) in which the

relative positions of the points approximately preserve the relationships between the spectra, thereby providing a more easily comprehended representation. Since the method focuses on interpoint distances, within such plots the choice of the axes is arbitrary and the distribution of points can be arbitrarily rotated or translated in unison within the lower dimensional space. Further details may be found in references 34 and 35. The spectra separate into clusters corresponding to different structure classes (as determined mostly by X-ray or NMR for proteins with well-defined native folds and UVCD and/or NMR for polypeptides and natively unfolded proteins). The orientation of the axes has been chosen so as to provide a display with increasing α-helix content to the right, increasing *β*-sheet content to the left, and increasing disordered or irregular structure (in effect structure containing no extended α-helix or *β*-sheet) from top to bottom. The polypeptide and protein positions are color coded with respect to the seven different structure classes listed on the figure, which provide a useful initial classification that also follows naturally from the 2D NLM clustering. Since the α-helix and *β*-sheet contents are inversely correlated (the larger the amount of one, the smaller the amount of the other), the dimension 1 values associated with α-helix and *β*-sheet have opposite signs. The dimension 2 values associated with disordered/irregular structure and the total amount of α-helix and *β*-sheet are similarly inversely correlated (the larger the amount of secondary structure, helix or sheet or both, the smaller the amount of disordered/irregular structure). Disordered/irregular sequences may adopt any structure other than α-helix or *β*-sheet, including PPII helix, turns, and unassociated *β*-strand. The positions of the four murine PrP^{23-231} samples, which are marked in Figure 3, provide information about their structures relative to each other and to those of the other proteins in the data set. Reassuringly, the metal-free PrP (*1*) falls at the boundary between the mainly α and the mainly irregular/disordered regions, consistent with its known solution NMR structure containing a folded mainly α C-terminal domain with only a small amount of *β*-sheet, and an unfolded N-terminal domain. Refolded murine PrP^{23-231} to which Cu^{2+} ions have been added (*2*) falls toward the top of the mainly disordered/irregular region and a little to the left of the vertical center line, which suggests that the lost α-helical structure is replaced with *β*-like structure. The PrP refolded in the presence of Cu^{2+} (*3*) is located lower down within the all-disordered/irregular region and considerably to the left of the vertical center line, which implies a bias toward *β*-like structure. The PrP refolded in the presence of Mn^{2+} (*4*) is situated above the metal-free PrP (*1*), comfortably within the all-α region and consistent with the appearance of its ROA spectrum, which reveals increased α-helix at the expense of PPII structure.

We also prepared a mutant (null-his PrP^{23-231}) in which the first six histidines located in the N-terminal sequence, and which are responsible for binding Cu^{2+} ions, are replaced by alanine in order to confirm that, without the copper binding sites, refolding in the presence of Cu^{2+} generates a structure similar to that of the wild type. Unfortunately, due to problems with a high Raman background, we were unable to measure its ROA spectrum after refolding with and without Cu^{2+}. However, we were able to measure the corresponding UVCD spectra (vide infra).

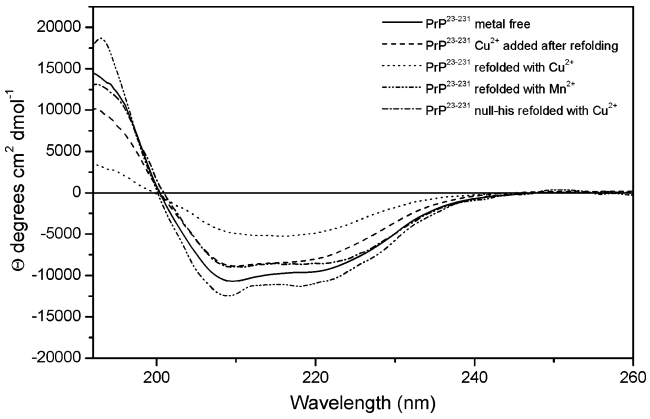

FIGURE 4: Far-UV CD spectra of the recombinant murine PrP^{23-231} samples in aqueous solution.

UV CD Data. The far-UV CD spectra of the four murine PrP^{23-231} samples discussed above, together with that of null-his PrP^{23-231} refolded with Cu^{2+}, are displayed in Figure 4. The shapes of all five spectra are similar, but the molar ellipticity amplitudes are very different in some cases. Only α-helix contents are reported from the secondary structure analysis since the analysis of *β*-sheet contents tends to be much less accurate than those of α-helix when significant amounts of α-helix are present (spectral contributions from helices and sheets above 190 nm are overlapping with the intense signal from α-helix dominating the spectrum) (*36*). The secondary structure analysis provides a total α-helix content of ∼25% for metal-free murine PrP^{23-231}, the same as that found in the PDB solution NMR structure 1dx0 of the full-length bovine prion protein.

The total α-helix content found for murine PrP^{23-231} when Cu^{2+} ions are added after refolding is ∼18%. This is consistent with the corresponding ROA spectrum, Figure 2b, which reveals significant loss of the hydrated (but not the unhydrated) α-helix. The associated small reduction observed in the amplitude of the far-UV CD spectrum is very similar to that reported previously on addition of Cu^{2+} ions to refolded full-length hamster PrP (*37*).

When murine PrP^{23-231} is refolded in the presence of Cu^{2+}, a dramatic decrease in the amplitude of the far-UV CD spectrum is observed. The associated total α-helix content is found to be only ∼5%, consistent with the appearance of the ROA spectrum, Figure 2c. The shape of the spectrum is consistent with an increase in *β*-sheet content. Refolding in the presence of Mn^{2+}, on the other hand, generates a far-UV CD spectrum with increased amplitude compared to that of the metal-free protein. The corresponding total α-helix content is now found to have increased to ∼30%, consistent with the appearance of the ROA spectrum, Figure 2d, which indicates an increase in α-helical structure.

The far-UV CD spectrum of null-his PrP^{23-231} refolded in the presence of Cu^{2+} ions reveals an α-helix content of ∼23%, which is similar to that of the wild-type metal-free protein (∼25%) suggesting that, without the histidine metal-binding sites, the presence of Cu^{2+} does not perturb the secondary structure significantly during refolding. We also prepared a sample of the null-his PrP refolded in the absence of Cu^{2+}, but problems with light scattering prevented measurement of its CD spectrum below ∼200 nm. However, down to this wavelength its CD spectrum (not shown) was

essentially superimposable on that of the null-his PrP refolded in the presence of Cu^{2+}, which suggests a similar secondary structure composition and also that the scattering did not significantly distort the CD data above ~200 nm.

The near-UV CD spectrum of our sample of metal-free murine PrP^{23-231} (not shown) is very similar to previously published spectra of prion proteins (*37*). It changes in exactly the same way on addition of Cu^{2+} after refolding (*37*), showing an additional band in the aromatic region indicative of a change in the tertiary structural environment of the aromatic residues. The near-UV CD spectrum of the PrP refolded in the presence of Cu^{2+} shows an even greater change in the aromatic region, whereas the protein refolded in the presence of Mn^{2+} ions shows very little change, thereby reinforcing the conclusion from the ROA and the far-UV CD data that Cu^{2+} significantly alters the fold but Mn^{2+} does not.

The Different Influences of Cu^{2+} and Mn^{2+} on PrP Folding. Both the ROA and UV CD data independently suggest that binding of Cu^{2+} and Mn^{2+} ions have dramatically different effects on the structure of murine PrP^{23-231}. In particular, PrP appears to fold differently depending on the methodology used to incorporate copper. Another recent study using dual polarization interferometry has also provided evidence that copper incorporation can result in two seemingly distinct conformations (*38*). The first, generated by copper incorporation during refolding, has an elongated structure; while the second, generated by copper incorporation after refolding, is slightly shorter and denser. Which of these two possible conformations is present in vivo would depend on when copper incorporation occurs in the cell. Given the high affinity for Cu^{2+} reported for this protein (*21*), it is likely that some copper would be incorporated during synthesis and entry into the endoplasmic reticulum. This would imply that the more unfolded structure would predominate. However, if PrP reached the cell surface without copper binding, then the second, more helical structure would be found.

The far-UV CD data reveal that adding Cu^{2+} to the already refolded PrP results in a drop in total α-helix content from ~25% to ~18%, accompanied by some change in tertiary structure, with the ROA data providing the additional insight that this loss occurs almost exclusively within the hydrated helix sequences. Refolding of the PrP in the presence of Cu^{2+}, on the other hand, has a more dramatic effect: despite the fact that the single C-terminal disulfide bond still forms (*39*), most of the α-helix is lost, with only ~5% remaining according to far-UV CD. The NLM analysis of the ROA data indicates a mainly disordered/irregular structure with a bias toward some β-like structure. Similarly the far-UV CD data suggest a mainly β-sheet and irregular structure. Why refolding murine PrP^{23-231} in the presence of Cu^{2+} should generate a structure comprising mainly irregular sequences in both N- and C-terminal regions, whereas adding Cu^{2+} ions to the PrP after refolding destabilizes/unfolds only the hydrated α-helix structure within the C-terminal region, remains an open question. It could be relevant that copper−copper interactions have been detected at full copper occupancy (*40*), suggesting that the octarepeat domain partially collapses.

The large positive−negative−positive triplet band pattern in the range ~1020−1140 cm^{-1} in the ROA spectrum of metal-free murine PrP^{23-231} (Figure 2a) is completely absent in the ROA spectra of the copper-bound proteins (parts b and c of Figure 2), suggesting that binding of Cu^{2+} completely changes the conformation of the corresponding sequence. The pattern is not characteristic of an α-helical domain nor is it likely to originate in or below the octarepeat region since it is perceptible in the ROA spectrum of ovine PrP^{94-233} (*32*). (The only other protein in our dataset displaying a very similar ROA band pattern in this wavenumber range is the α + β protein ribonuclease A, shown in reference 23, which contains an unusually long stretch of highly twisted β-strand that contributes to two separate short stretches of double-stranded β-sheet.) It is therefore likely that this triplet originates in the region ~90−170, at the beginning of which two additional putative copper binding sites, His^{95} and His^{110}, have been identified (*18*, *19*). Referring to the NMR solution structure of murine $PrP^{121-231}$ in Figure 1, this region contains a short segment of double-stranded antiparallel β-sheet (129−130, 162−163) with a stretch of α-helix (α-helix 1, residues 145−156) forming part of the long loop connecting the ends of the two β-strands. Consequently, we could speculate that the hydrated α-helix that is lost or modified when Cu^{2+} ions are added after refolding corresponds to α-helix 1. As in the present study, a ^1H NMR study of copper binding to the full-length prion protein also reported that copper binding to the N-terminal domain, albeit under mildly acidic conditions, leads to some interaction with the C-terminal domain, including signal reductions near the C-terminal end of this helix (*41*). Another study reported this helix to be extremely hydrophilic with very low protection factors toward hydrogen−deuterium exchange (*42*).

Our results suggest that, unlike binding of Cu^{2+}, which disrupts α-helix and the associated C-terminal folded domain of murine PrP^{23-231}, binding of Mn^{2+} reinforces the α-helix content. Thus our far-UV CD data reveal that, on refolding the PrP in the presence of Mn^{2+}, the α-helix content increases from ~25% to ~30%, with our ROA data indicating that this extra α-helix is formed from sequences, possibly PPII-like, in the unfolded N-terminal region. A possible explanation for this different behavior might be found in the distinct coordination and hydration characteristics of Cu^{2+} and Mn^{2+} ions. The X-ray crystal structure of HGGGW, which comprises the fundamental copper binding unit within an octarepeat, in a complex with Cu^{2+} reveals the metal ion to be bound in a square pyramidal complex to the histidine imidazole, to two deprotonated glycine amides, and to a glycine carbonyl, along with an axial water bridging to the tryptophan indole (*12*,*43*). (This only appears to be obtained at full copper occupancy: low copper occupancy favors different coordination modes (*12*, *40*).) According to the Irving−Williams series, which summarizes the relative stabilities of complexes formed by M^{2+} ions of the 3d transition metal series and reflects a combination of electrostatic effects and ligand field stabilization energies (*44*), the stability constants of complexes are much greater for Cu^{2+} than for Mn^{2+}, which shows no great propensity to complex with N-donors while Cu^{2+} does. Furthermore, Mn^{2+} forms regular octahedral complexes, but Cu^{2+} prefers square planar or square pyramidal complexes (*44*). Hence Cu^{2+} will bind strongly to the HGGGW binding site, as observed (*43*), thereby greatly perturbing the PrP structure; while Mn^{2+} is

expected to bind only weakly, if at all, to this site. Rather, Mn^{2+} is expected to form less strong associations with PrP, with weakly coordinated water molecules completing the hexacoordination and perhaps also serving to further stabilize hydrated α-helix structure. This idea is supported by the X-ray crystal structure of manganese-bound T7 endonuclease I in which Mn^{2+} is observed to bind to three protein ligands at one site and a single protein ligand at a second site, with the hexacoordination of the ion completed by a corresponding number of water molecules (*45*). Further supporting evidence arises from NMR and electron paramagnetic resonance (EPR) studies of a synthetic peptide corresponding to the human $PrP^{106-126}$ sequence which revealed different binding regions and coordination modes for Cu^{2+} and Mn^{2+} at pH 5.7, with the latter forming a six-coordinate octahedral complex involving Gly^{126}, Leu^{125}, Gly^{124}, and His^{111}, a hydrogen bond of metal-bound water most likely being involved in the interaction with the imidazole ring of His^{111} (*46*).

Manganese has been reported to favor the formation of proteinase-resistant PrP (*15*,*16*). In studies with the recombinant protein this process requires incubation (*15*). Previous studies have also shown that binding of manganese initially results in the formation of increased helical content in the protein (*15*). However, under certain conditions such as exposure to infrared radiation (*47*), this helical structure is destabilized and the protein undergoes a gradual structural transition resulting in increased *β*-sheet content that can result in aggregation (*15*).

CONCLUSIONS

This combined ROA and UV CD study has reinforced earlier indications that the binding of metal ions may influence the structure of prion proteins, with detailed results on binding of Cu^{2+} and Mn^{2+} to full-length murine PrP^{23-231} revealing that these particular ions can affect the global structure more profoundly than previously thought. Remarkably, although Cu^{2+} tends to destroy the α-helix, partially when added after refolding and almost completely if present during refolding, Mn^{2+} reinforces it. The tentative suggestion from our data that addition of Cu^{2+} after refolding selectively disrupts the region ∼90−170 containing α-helix 1 is especially interesting since this corresponds to the region which immunologic studies of PrP^{Sc} indicate is mostly involved in the conversion of PrP^{C} into PrP^{Sc} (*48*,*49*), with secondary structure changes located in α-helix 1 (*50*). It is also the region suggested to form left-handed *β*-helices in a model of PrP^{Sc}, with the rest of the C-terminal region retaining the disulfide-linked α-helices 2 and 3 observed in PrP^{Sc} (*51*).

Although our studies were carried out on recombinant (carbohydrate-free) murine PrP^{23-231}, the NMR solution structure of naturally occurring bovine PrP^{23-230} containing the two carbohydrate moieties revealed that the three-dimensional structure and thermal stability of the natural glycoprotein and the recombinant carbohydrate-free protein are essentially identical (*52*). However, it is well-known that carbohydrates coordinate with metal ions in general and Cu^{2+} in particular (*53*). Furthermore, the prion protein is a sialoglycoprotein (*54*), and Cu^{2+} forms well-characterized coordination species with sialic acid (*55*). The possibility that glycosylation in the naturally occurring protein could modulate the uptake of metal ions should therefore be kept in mind.

In summary, as well as revealing new structural aspects of the binding of divalent copper and manganese ions that could be important in the normal cellular function of prion proteins, our results also show that there is ample scope for these and possibly other metal ions to be involved in misfunction and associated TSE disease, with possible implications for the development of TSE chemotherapeutics (*4*).

REFERENCES

1. Prusiner, S. B. (1998) Prions, *Proc. Natl. Acad. Sci. U.S.A. 95*, 13363−13383.
2. Cohen, F. E., and Prusiner, S. B. (1998) Pathologic conformations of prion proteins, *Annu. Rev. Biochem. 67*, 793−819.
3. Surewicz, W. K., Jones, E. M., and Apetri, A. C. (2006) The Emerging Principles of Mammalian Prion Propagation and Transmissibility Barriers: Insight from Studies in Vitro, *Accs. Chem. Res. 39*, 654−662.
4. Caughey, B., Caughey, W. S., Kocisko, D. A., Lee, K. S., Silveira, J. R., and Morrey, J. D. (2006) Prions and Transmissible Spongiform Encephalopathy (TSE) Chemotherapeutics: A Common Mechanism for Anti-TSE Compounds, *Acc. Chem. Res. 39*, 646−653.
5. Pan, K. M., Baldwin, M., Nguyen, J., Gasset, M., Serban, A., Groth, D., Mehlhorn, I., Huang, Z., Fletterick, R. J., Cohen, F. E., and Prusiner, S. B. (1993) Conversion of α-helices into *β*-sheets features in the formation of the scrapie prion proteins, *Proc. Natl. Acad. Sci. U.S.A. 90*, 10962−10966.
6. Pergamini, P., Jaffe, H., and Safar, J. (1996) Semipreparative chromatographic method to purify the normal cellular isoform of the prion protein in nondenatured form, *Anal. Biochem. 236*, 63−73.
7. Wüthrich, K., and Riek, R. (2001) Three-dimensional structures of prion proteins, *Adv. Prot. Chem. 57*, 55−82.
8. Haire, L. F., Whyte, S. M., Vasisht, N., Gill, A. C., Verma, C., Dodson, E. J., Dodson, G. G., and Bayley, P. M. (2004) The crystal structure of the globular domain of sheep prion protein, *J. Mol. Biol. 336*, 1175−1183.
9. Brown, D. R. (1999) Prion protein expression aids cellular uptake and veratridine-induced release of copper, *J. Neurosci. Res. 58*, 717−725.
10. Brown, D. R., Wong, B.-S., Hafiz, F., Clive, C., Haswell, S., and Jones, I. M. (1999) Normal prion protein has superoxide dismutase-like activity, *Biochem. J. 344*, 1−5.
11. Brown, D. R., Clive, C., and Haswell, S. (2001) Anti-oxidant activity related to copper binding of native prion protein, *J. Neurochem. 76*, 69−76.
12. Millhauser, G. L. (2006) Copper and the prion protein: methods, structures, function, and disease, *Ann. Rev. Phys. Chem. 58*, 299−320.
13. Wong, B.-S., Chen, S. G., Colucci, M., Xie, Z., Pan, T., Liu, T., Li, R., Gambetti, P., Sy, M.-S., and Brown, D. R. (2001) Aberrant metal binding by prion protein in human prion protein disease, *J. Neurochem. 78*, 1400−1408.
14. Thackray, A. M., Knight, R., Haswell, S. J., Bujdoso, R., and Brown, D. R. (2002) Metal imbalance and compromised antioxidant function are early changes in prion disease, *Biochem. J. 362*, 253−258.
15. Brown, D. R., Hafiz, F., Glasssmith, L. L., Wong, B.-S., Jones, I. M., Clive, C., and Haswell, S. J. (2000) Consequences of manganese replacement of copper for prion protein function and proteinase resistance, *EMBO J. 19*, 1180−1186.
16. Treiber, C., Simons, A., and Multhaup, G. (2006) Effect of copper and manganese on the de novo generation of protease-resistant prion protein in yeast cells, *Biochemistry 45*, 6674−6680.
17. Viles, J. H., Cohen, F. E., Prusiner, S. B., Goodin, D. B., Wright, P. E., and Dyson, H. J. (1999) Copper binding to the prion protein: Structural implications of four identical cooperative binding sites, *Proc. Natl. Acad. Sci. U.S.A. 96*, 2042−2047.
18. Jones, C. E., Abdelraheim, S. R., Brown, D. R., and Viles, J. H. (2004) Preferential Cu^{2+} coordination by His^{96} and His^{111} induces *β*-sheet formation in the unstructured amyloidogenic region of the prion protein, *J. Biol. Chem. 279*, 32018−32027.

19. Jones, C. E., Klewpatinond, M., Abdelraheim, S. R., Brown, D. R., and Viles, J. H. (2005) Probing copper^{2+} binding to the prion protein using diamagnetic nickel^{2+} and ^{1}H NMR: the unstructured N terminus facilitates the coordination of six copper^{2+} ions at physiological concentrations, *J. Mol. Biol. 346*, 1393−1407.
20. Burns, C. S., Aronoff-Spencer, E., Legname, G., Prusiner, S. B., Antholine, W. E., Gerfen, G. J., Peisach, J., and Millhauser, G. L. (2003) Copper coordination in the full-length, recombinant prion protein, *Biochemistry 42*, 6794−6803.
21. Thompsett, A. R., Abdelraheim, S. R., Daniels, M., and Brown, D. R. (2005) High affinity binding between copper and full-length prion protein identified by two different techniques, *J. Biol. Chem. 280*, 42750−42758.
22. Bradford, M. M. (1976) A rapid and sensitive method for the quantitation of microgram quantities of protein utilizing the principle of protein-dye binding, *Anal. Biochem. 72*, 248−254.
23. Zhu, F., Isaacs, N. W., Hecht, L., and Barron, L. D. (2005) Raman optical activity: a tool for protein structure analysis, *Structure 13*, 1409−1419.
24. StatSoft Inc. *STATISTICA* (data analysis software system), version 6, 2004. http://www.statsoft.com.
25. Kelly, S. M., Jess, T. J., and Price, N. C. (2005) How to study proteins by circular dichroism, *Biochim. Biophys. Acta 1751*, 119−139.
26. Sreerama, N., and Woody, R. W. (2000) Estimation of protein secondary structure from CD spectra: Comparison of CONTIN, SELCON and CDSSTR methods with an expanded reference set, *Anal. Biochem. 287* (2), 252−260.
27. Whitmore, L., and Wallace, B. A. (2004) DICHROWEB: an online server for protein secondary structure analyses from circular dichroism spectroscopic data, *Nucleic Acids Res. 32*, W668−673.
28. Barron, L. D. (2004) *Molecular Light Scattering and Optical Activity*, 2nd ed., Cambridge University Press, Cambridge.
29. Barron, L. D. (2006) Structure and behaviour of biomolecules from Raman optical activity, *Curr. Opin. Struct. Biol. 16*, 638−643.
30. McColl, I. H., Blanch, E. W., Gill, A. C., Rhie, A. G. O., Ritchie, M. A., Hecht, L., Nielsen, K., and Barron, L. D. (2003) A new perspective on β-sheet structures using vibrational Raman optical activity: from poly(L-lysine) to the prion protein, *J. Am. Chem. Soc. 125*, 10019−10026.
31. McColl, I. H., Blanch, E. W., Hecht, L., and Barron, L. D. (2004) A study of α-helix hydration in polypeptides, proteins and viruses using vibrational Raman optical activity, *J. Am. Chem. Soc. 126*, 8181−8188.
32. Blanch, E. W., Gill, A. C., Rhie, A. G. O., Hope, J., Hecht, L., Nielsen, K., and Barron, L. D. (2004) Raman optical activity demonstrates poly(L-proline) II helix in the N-terminal region of the ovine prion protein: implications for function and misfunction, *J. Mol. Biol. 343*, 467−476.
33. McColl, I. H., Blanch, E. W., Hecht, L., Kallenbach, N. R., and Barron, L. D. (2004) Vibrational Raman optical activity characterization of poly(L-proline) II helix in alanine oligopeptides, *J. Am. Chem. Soc. 126*, 5076−5077.
34. Zhu, F., Tranter, G. E., Isaacs, N. W., Hecht, L., and Barron, L. D. (2006) Delineation of protein structure classes from multivariate analysis of protein Raman optical activity data, *J. Mol. Biol. 363*, 19−26.
35. Zhu, F., Kapitan, J., Tranter, G. E., Pudney, P. D. A., Isaacs, N. W., Hecht, L., and Barron, L. D. (2008) Residual structure in disordered peptides and unfolded proteins from multivariate analysis and ab initio simulation of Raman optical activity data, *Proteins*, *70*, 823−833.
36. Wallace, B. A., and Janes, R. W. (2001) Synchrotron radiation circular dichroism spectroscopy of proteins: secondary structure, fold recognition and structural genomics, *Curr. Opin. Chem. Biol. 5*, 567−571.
37. Stöckel, J., Safar, J., Wallace, A. C., Cohen, F. E., and Prusiner, S. B. (1998) Prion protein selectively binds copper(II) ions, *Biochemistry 37*, 7185−7193.
38. Thompsett, A. R., and Brown, D. R. (2007) Dual polarisation interferometry analysis of copper binding to the prion protein: evidence for two folding states, *Biochim. Biophys. Acta 1774*, 920−927.
39. Wong, B.-S., Vénien-Bryan, C., Williamson, R. A., Burton, D. R., Gambetti, P., Sy, M.-S., Brown, D. R., and Jones, I. M. (2000) Copper refolding of prion protein, *Biochem. Biophys. Res. Commun. 276*, 1217−1224.
40. Chattopadhyay, M., Walter, E. D., Newell, D. J., Jackson, P. J., Aronoff-Spencer, E., Peisach, J., Gerfen, G. J., Bennett, B., Antholine, W. E., and Millhauser, G. L. (2005) The octarepeat domain of the prion protein binds Cu(II) with three distinct coordination modes at pH 7.6, *J. Am. Chem. Soc. 127*, 12647−12656.
41. Wells, M. A., Jackson, G. S., Jones, S., Hosszu, L. L. P., Craven, C. J., Clarke, A. R., Collinge, J., and Waltho, J. P. (2006) A reassessment of copper(II) binding in the full-length prion protein, *Biochem. J. 399*, 435−444.
42. Calzolai, L., and Zahn, R. (2003) Influence of pH on NMR structure and stability of the human prion protein globular domain, *J. Biol. Chem. 278*, 35592−35596.
43. Burns, C. S., Aronoff-Spencer, E., Dunham, C. M., Lario, P., Avdievich, N. I., Antholine, W. E., Olmstead, M. M., Vrielink, A., Gerfen, G. J., Peisach, J., Scott, W. G., and Millhauser, G. L. (2002) Molecular features of the copper binding sites in the octarepeat domain of the prion protein, *Biochemistry 41*, 3991−4001.
44. Atkins, P., Overton, T., Rourke, J., Weller, M., and Armstrong, F. (2006) *Shriver and Atkins Inorganic Chemistry*, 4th ed., Oxford University Press, Oxford.
45. Hadden, J. M., Déclais, A.-C., Phillips, S. E. V., and Lilley, D. M. J. (2002) Metal ions bound at the active site of the junction-resolving enzyme T7 endonuclease I, *EMBO J. 21*, 3505−3515.
46. Gaggelli, E., Bernardi, F., Molteni, E., Pogni, R., Valensin, D., Valensin, G., Remelli, M., Luczkowski, M., and Kozlowski, H. (2005) Interaction of the human prion PrP(106−126) sequence with copper(II), manganese(II), and zinc(II): NMR and EPR studies, *J. Am. Chem. Soc. 127*, 996−1006.
47. Tsenkova, R. N., Iordinova, I. K., Toyoda, K., and Brown, D. R (2004) Prion protein fate governed by metal binding, *Biochem. Biophys. Res. Commun. 325*, 1005−1012.
48. Peretz, D., Williamson, R. A., Matsunaga, Y., Serban, H., Pinilla, C., Bastidas, R. B., Rozenshteyn, R., James, T. L., Houghten, R. A., Cohen, F. E., Prusiner, S. B., and Burton, D. R. (1997) A conformational transition at the N terminus of the prion protein features in formation of the scrapie isoform, *J. Mol. Biol. 273*, 614−622.
49. Korth, C., Stierli, B., Streit, P., Moser, M., Schaller, O., Fischer, R., Schulz-Schaeffer, W., Kretzschmar, H., Raeber, A., Braun, U., Ehrensperger, F., Hornemann, S., Glockshuber, R., Riek, R., Billeter, M., Wüthrich, K., and Oesch, B. (1997) Prion (PrP^{Sc})-specific epitope defined by a monoclonal antibody, *Nature 389*, 74−77.
50. Eghiaian, F., Grosclaude, J., Lesceu, S., Debey, P., Doublet, B., Tréguer, E., Rezaei, H., and Knossow, M. (2004) Insight into the $PrP^{C} \rightarrow PrP^{Sc}$ conversion from the structures of antibody-bound ovine prion scrapie-susceptibility variants, *Proc. Natl. Acad. Sci. U.S.A. 101*, 10254−10259.
51. Govaerts, C., Wille, H., Prusiner, S. B., and Cohen, F. E. (2004) Evidence for assembly of prions with left-handed β-helices into trimers, *Proc. Natl. Acad. Sci. U.S.A. 101*, 8342−8347.
52. Hornemann, S., Schorn, C., and Wüthrich, K. (2004) NMR structure of the bovine prion protein isolated from healthy calf brains, *EMBO Rep. 5*, 1159−1164.
53. Gyurcsik, B., and Nagy, L. (2000) Carbohydrates as ligands: coordination equilibria and structure of the metal complexes, *Coord. Chem. Rev. 203*, 81−149.
54. Bolton, D. C., Meyer, R. K., and Prusiner, S. B. (1985) Scrapie PrP 27−30 is a sialoglycoprotein, *J. Virol. 53*, 596−606.
55. Fainerman-Melnikova, M., Szabó-Plánka, T., Rockenbauer, A., and Codd, R. (2005) Coordination modes between copper (II) and N-acetylneuraminic (sialic) acid from a 2D simulation analysis of EPR spectra. Implications for copper mediation of sialoglyco-conjugate chemistry relevant to human biology, *Inorg. Chem. 44*, 2531−2543.

BI7022893